

RESEARCH ARTICLE

The potential role of the SIRT1-Nrf2 signaling pathway in alleviating hidden hearing loss via antioxidant stress

Zeyu Zheng^{1,2} | Peng Zhang³ | Yang Fu^{1,2} | Yihong Jiang^{1,2} | Jing Zhu^{1,2} |
Fei Wang⁴ | Shaoheng Li⁵ | Zhuoru Zhang^{1,2} | Tong Chang^{1,2} | Tian Li⁶  |
Min Zhang^{1,3} | Bai Ruan^{1,2} | Xiaocheng Wang^{1,2} 

¹Center of Clinical Aerospace Medicine, School of Aerospace Medicine, Key Laboratory of Aerospace Medicine of Ministry of Education, Air Force Medical University, Xi'an, Shaanxi, China

²Department of Aviation Medicine, Xijing Hospital, Xi'an, China

³Department of Otolaryngology, Xijing Hospital, Xi'an, China

⁴School of Basic Medicine, Air Force Medical University, Xi'an, China

⁵Department of Ophthalmology, Eye Institute of Chinese PLA, Xijing Hospital, Xi'an, China

⁶Tianjin Medical University, Tianjin, China

Correspondence

Xiaocheng Wang, Min Zhang, and Bai Ruan, Center of Clinical Aerospace Medicine, School of Aerospace Medicine, Key Laboratory of Aerospace Medicine of Ministry of Education, Air Force Medical University, Xi'an 710032, China.

Email: wxcnose@126.com, zhangmin2015@fmmu.edu.cn and bairuan@fmmu.edu.cn

Funding information

Health care special scientific research project of Health Bureau, Logistics Support Department, CMC, Grant/Award Number: 17BJZ24; Military Medical Talents Support Fund of "Mount Everest Project" of Air Force Medical University, Military logistics scientific research standard, Grant/Award Number: BKJ19B045; National Natural Science Foundation of China, Grant/Award Number: 82373610

Abstract

Hidden hearing loss (HHL) is characterized by normal audiometric thresholds but impaired auditory function, particularly in noisy environments. In vivo, we employed auditory brainstem response (ABR) testing and ribbon synapses counting to assess changes in mouse hearing function, and observed the morphology of hair cells through scanning electron microscopy. SRT1720 was administered to the cochlea via round window injection. In vitro, western blot analysis and RT-qPCR were used, and Lenti-shNrf2 was used to knockdown Nrf2 expression. In addition, various oxidative stress indicators were detected by immunofluorescence, kit-based assays, and flow cytometry. ABR measurement of HHL mouse showed a significant increase in hearing threshold, as well as a decrease and delay in the I wave amplitude and latency on the first day after noise exposure. Histological observation showed a significant loss of ribbon synapses and stereocilia lodging. HHL mice exhibited oxidative stress, which was reduced by pretreatment with SRT1720. Additionally, SRT1720 could reduce hydrogen peroxide-induced oxidative stress in HEI-OC1 cells through activating the SIRT1/Nrf2 pathway. Subsequent experiments with Nrf2 knockdown confirmed the importance of this pathway. Findings highlight oxidative stress as the primary contributor to HHL, with the SIRT1/Nrf2 signaling pathway emerging as a promising therapeutic target for alleviating HHL.

KEYWORDS

hidden hearing loss, Nrf2, oxidative stress, ribbon synapses, SRT1720

Zeyu Zheng, Peng Zhang, and Yang Fu contributed equally to this study.

This is an open access article under the terms of the [Creative Commons Attribution-NonCommercial-NoDerivs](https://creativecommons.org/licenses/by-nc-nd/4.0/) License, which permits use and distribution in any medium, provided the original work is properly cited, the use is non-commercial and no modifications or adaptations are made.

© 2024 The Author(s). *Cell Biology International* published by John Wiley & Sons Ltd on behalf of International Federation of Cell Biology.

1 | INTRODUCTION

Hidden hearing loss (HHL) is a recently proposed subtype of sensorineural hearing loss (SNHL) characterized by maintained audiometric thresholds, but a significant decrease in auditory perceptual function, particularly in understanding speech in noisy environments (Kohrman et al., 2020). This condition is primarily caused by the loss of ribbon synapses between the inner hair cells and auditory nerve fibers, as opposed to defects in the central auditory pathways or degeneration of hair cells seen in other forms of SNHL. Early intervention at this stage can potentially prevent further progression of hearing impairment (Liu et al., 2024). Therefore, conducting basic research to identify the pathogenesis of HHL and developing targeted interventions for this specific type of hearing loss is imperative.

The pathogenesis of HHL remains poorly understood. However, emerging research has indicated that disturbances in free radical homeostasis and oxidative stress play significant roles in the onset and progression of HHL (Tan & Song, 2023). The high metabolic demands of the cochlea render its tissues, particularly the inner hair, outer hair, and spiral ganglion cells, more vulnerable to damage caused by mitochondrial reactive oxygen species (ROS). The accumulation of excessive ROS can result in oxidative damage to crucial mitochondrial components, such as mitochondrial DNA, mitochondrial membranes, and respiratory chain proteins. This leads to mitochondrial dysfunction, where the mitochondria fail to meet the high metabolic requirements of the cochlea. Consequently, this may contribute to noise-induced hearing loss (NIHL), tinnitus, and acoustic hyperesthesia.

While our previous studies have shown the protective effects of resveratrol on HHL in guinea pigs via the SIRT1/PGC-1 α pathway, the factors exacerbating HHL in the more commonly used experimental animal, C57BL/6J mice, remain poorly understood. In addition, for the future treatment of HHL, understanding the specific molecular pathways involved is crucial. Therefore, we aimed to establish an *in vivo* model of HHL in C57BL/6J mice and an *in vitro* model of oxidative stress in hydrogen peroxide (H₂O₂)-induced House Ear Institute Organ of Corti (HEI-OC1) cells to study the exacerbation of HHL. Subsequently, we sought to use the SIRT1-specific agonist SRT1720 to investigate the molecular mechanisms involved in mitigating the progression of HHL, both *in vivo* and *in vitro*.

2 | MATERIALS AND METHODS

2.1 | Animal groups

Six-week-old male C57BL/6J mice (Schubert et al., 2024) were purchased from the Laboratory Animal Center of Air Force Medical University. None of the mice had prior exposure to noise. All mice underwent a 1-week acclimatization period and were housed in a temperature-controlled room at 22 \pm 2°C, with a 12 h light/dark cycle, and *ad libitum* access to food and water. ABR testing was conducted on all mice before the experiment. The mice were randomly assigned to four groups of 6 mice each: a control (CON) group

receiving no treatment; a NE group exposed to 110 dB SPL noise for 2 h while awake; a SRT1720 + NE (SRT + NE) group administered SRT1720 (HY-10532, MedChemExpress) at a dose of 10 mM, with 10 μ L per cochlea via round-window injection and exposed to noise after 2 h; and a vehicle (VEHL) group receiving only round-window injection of vehicle (6.67% DMSO in PBS), at 10 μ L per cochlea. All procedures performed in this study were approved by the Institutional Animal Care and Use Committee of Xi'an Air Force Medical University, China (No.20230375).

2.2 | Noise stimulation and procedure

The noise utilized was broadband noise and obtained from a specific type of military helicopter. The noise consisted of engine and rotor noise and was played through a loudspeaker (IT-12, RADIN, CHN) using an amplifier (AV-502BT, BGL, CHN) for loop playback. NE took place in a soundproof chamber with mice housed in a mouse cage (10.5 cm \times 5.5 cm \times 5.5 cm); the loudspeakers were positioned on both sides of the cage. The intensity of the noise was measured using A-weighted sound level (HCJYET HT8352, CHN) to ensure that the difference in sound pressure level within the mice's activity area was less than 3 dB SPL. Mice in the NE group and SRT + NE group were exposed to 110 dB SPL noise for 2 h while awake, the CON group were placed in an identical environment but did not receive any NE (Yihong et al., 2024); ambient background noise remained below 15 dB SPL.

2.3 | ABR measurements

All mice in this experiment were required to undergo ABR testing prior NE and 1 d after NE. The mice were anesthetized by intraperitoneal injection of 1% pentobarbital sodium (0.3 mL/100 g) combined with Xylazine Hydrochloride (0.04 mL), and if the animals did not return to the lying position when placed laterally, the mice were fully anesthetized. After satisfactory anesthesia, the recording electrode was placed under the skin at the midpoint between the two ears of the mouse, while the reference electrode was placed under the skin behind the test ear, and a ground electrode was inserted into the base of each mouse's tail. In this study, a short sound stimulus (Click) and pure tone at 1, 2, 4, and 8 kHz were used for ABR testing, with stimulus intensity starting from 80 dB SPL and decreasing at 5 dB SPL intervals. The hearing threshold of each mouse was determined as being at its lowest stimulus intensity for wave III. Simultaneously, both amplitude and latency of wave I at 80 dB SPL were recorded. The mice with ABR threshold below 10 dB SPL were selected as subjects for the experiment.

2.4 | Round-window injection

For the round-window injection in adult mice, 6-week-old male C57BL/6J mice were utilized. Before surgery, the mice were

anesthetized with a combination of 1% pentobarbital sodium (0.3 mL/100 g) and Xylazine Hydrochloride (0.04 mL). Skin disinfection was carried out using 75% alcohol, gently removing hair behind both ears to expose the skin. The mouse was positioned on its side on a dissecting table, and then the skin was cut along the ear boundary furrow at the back and bottom of the external auditory canal, separated subcutaneous tissues, and exposed the otic bulla. A microdrill was used to create a small hole in the otic bulla for injections performed through a 10 μ L glass micropipette. The wound was filled with hemostatic sponge and closed using 4-0 absorbable suture. Subsequently, mice were transferred to an electric blanket, keeping their injected ear up while lying on their side for 40 min, and then exposed to the noise after the mice fully recovered from anesthesia.

2.5 | Tissue preparation

Following ABR determination, the selected animals was placed in the euthanasia box, opened the CO₂ gas valve, once the animal loses consciousness, gradually increase the CO₂ concentration to 100%. When observed dystonia and no corneal reflex, the animal was continued to ventilate for 2 min to confirm its death. Afterward, mouse cochlear was extracted. The basilar membrane was meticulously prepared by delicately trimming excess bone and tissue. Subsequently, the samples were immersed in 4% paraformaldehyde at 4°C overnight. Post-fixation, the decalcification of the cochlear tissues was carried out using EDTA (PS0993-5, PSAITONG, CHN) for a duration of 3 d. The cochlear tissue was then transferred to PBS to remove any surplus tissue in preparation for isolating the basilar membrane from apex to base, intended for immunofluorescence staining.

2.6 | Ribbon synapse counting

The isolated cochlear basilar membranes were examined using a confocal microscope equipped with a 60 \times magnification oil immersion lens, and the emission wavelengths of 461 and 618 nm were utilized. Specific regions were selected for analysis at different locations (apex, middle, and base) within each basilar membrane. The quantification of ribbon synapses per inner hair cell was performed by tallying the total number of spots corresponding to CtBP2 staining and dividing this figure by the total immunoreactive spots observed in each field of view to determine the average number of ribbon synapses for each inner hair cell.

2.7 | Scanning electron microscope

The basilar membrane samples were initially cleaned with PBS to eliminate surface attachments, mucus, and impurities to achieve a clean observation surface. The cleaning solution and samples were gently shaken at a 1:20 volume ratio and then fixed with 3% glutaraldehyde. Following fixation, the samples underwent 3 washes

with PBS for 10 min each before being fixed with 1% osmic acid for 1 h. Subsequently, they were washed again three times with PBS for an additional 10 min each time. Next, the specimens were dehydrated using alcohol to replace the water in the tissues. This involved a concentration gradient of alcohol (30%, 50%, 70%, 80%, 90%, 95%, and 100%) where the highest concentration was repeated three times for a duration of 15 min each. Following dehydration, the samples were placed into a critical point dryer to prevent sample deformation. They were then affixed to a sample base using conductive adhesive and subjected to ion-sputtering treatment within an ion-sputtering instrument. Finally, images of the treated samples were captured using a scanning electron microscope (JSM-IT700HR, JPN). Specific areas of interest were selected for image collection.

2.8 | Cell culture and treatment

The House Ear Institute-Organ of Corti 1 (HEI-OC1) cells were cultured under permissive conditions at 33°C and 10% CO₂ in Dulbecco's Modified Eagle Medium (DMEM; PM150210, Procell, CHN) supplemented with 10% fetal bovine serum (FBS; 164210-50, Procell, CHN). The cells used were in the logarithmic growth phase and were seeded into 96-well plates at a density of 1×10^4 cells/well. For in vitro oxidative stress model establishment, the cells were treated with 50 μ M of H₂O₂ for a duration of 12 h. Additionally, SRT1720 was introduced at different concentrations (0, 1, 2, 4, 8 and 16 μ M) for a period of 12 h. A concentration that did not significantly affect cell viability and effectively reduced ROS levels was selected for further experimentation.

2.9 | Cell counting Kit-8 (CCK-8) assay

Following cell attachment, the cells were treated with various concentrations of SRT1720. Subsequently, 10 μ L of CCK-8 reagent (CK04, Dojindo, JPN) was added to each well and incubated at 37°C for 2 h. The absorbance of the samples was then measured at a wavelength of 450 nm.

2.10 | Transfections (Lenti-shNrf2)

HEI-OC1 cells were seeded in 96-well plates and incubated at 37°C. The cells were then infected with Lenti-shNrf2 (Hanbio, CHN) following the manufacturer's instructions. Puromycin was added to establish stable cell strains.

2.11 | Detection of superoxide dismutase (SOD), lipid peroxidation malondialdehyde (MDA), total antioxidant capacity (T-AOC) and ATP level

The SOD activity, lipid peroxidation MDA, total antioxidant capacity, and ATP level assays were performed using the following kits: the

total SOD assay kit with WST-8 (S0101S, Beyotime, CHN), the lipid peroxidation MDA assay kit (S0131S, Beyotime, CHN), the total antioxidant capacity assay kit with FRAP method (S0116, Beyotime, CHN), and the ATP content assay kit (BC0305, Solarbio, CHN). All procedures were carried out in accordance with the manufacturer's instructions. The chromaticity of each group was measured using a microplate reader equipped for colorimetry (BioTek) at 450 nm for SOD activity assessment, 532 nm for MDA levels determination, 593 nm for T-AOC evaluation, and 340 nm for ATP detection.

2.12 | Mitochondrial reactive oxygen species detection

Following the creation of different experimental groups, the Reactive Oxygen Species Assay Kit (E004-1-1, Jiancheng Biotechnology, CHN) was utilized to measure the level of ROS in these groups. According to the manufacturer's instructions, cells were stained with 10 μ L DCFH-DA at 37°C for 20 min. The fluorescence intensity of 2',7'-dichlorofluorescein (DCF) was then assessed using flow cytometry at an excitation wavelength of 488 nm and an emission wavelength of 525 nm.

2.13 | Mitochondrial potential detection (MMP)

To assess the Mitochondrial Membrane Potential (MMP), the MMP Assay Kit with Rhodamine 123 (C2008S, Beyotime, CHN) was utilized following the manufacturer's instructions. In brief, cells were incubated with rhodamine 123 at 37°C for 30 min. Subsequently, samples were rinsed twice with cell culture medium at 37°C and the results were evaluated using flow cytometry at an excitation wavelength of 507 nm and an emission wavelength of 529 nm.

2.14 | Immunofluorescence staining

Following the preparation of the basilar membrane, the samples were transferred into a 96-well plate. TritonX-100 at a concentration of 10 mL/L was applied for 1 h, followed by blocking using ready-to-use goat serum (AR0009 BOSTER, CHN). Subsequently, the samples were incubated overnight at 4°C with rabbit anti-CtBP2 antibody (ab128871, Abcam, UK, 1:100) and mouse anti-4 Hydroxynonenal (4-HNE) antibody (ab48506, Abcam, UK, 1:50) separately. The samples were then rinsed 3 times with PBS and incubated with secondary antibodies: cy3-conjugated affinipure goat anti-rabbit IgG (SA0009-2, Proteintech, USA, 1:200), and Goat polyclonal Secondary antibody to mouse IgG-H&L FITC (EK013, ZhuangzhiBiology, CHN, 1:100) for 2 h at room temperature. After incubation, the samples were washed three times with PBS before being transferred to glass slides and covered with a drop of antifade mounting medium containing DAPI (P0131, Beyotime, CHN). The results were observed under confocal microscopy (FV3000, Olympus JPN).

For cell samples, cultured cells in a special confocal petri dish (801002, Wuxi NEST Biotechnology CHN) before experimentation. Washed cells with PBS as they reached appropriate density, and fixed them using 4% paraformaldehyde. After fixation for 2 h, TritonX-100 at a concentration of 10 ml/L was used for 1 h, followed by blocking using ready-to-use goat serum. Then, Nrf2 polyclonal antibody (16396-1-AP Proteintech, USA, 1:100) was added, and the samples were incubated overnight. After adding secondary antibodies and antifade mounting medium containing DAPI, the images were able to be observed under confocal microscopy.

2.15 | Reverse transcriptase-quantitative polymerase chain reaction (RT-qPCR) analysis

Total RNA content was extracted using TRIzol reagent (15596018, Invitrogen, USA), followed by reverse transcription procedures performed with the assistance of MightyScript First Strand cDNA Synthesis Master Mix (B639251, Sangon Biotech, CHN). The primers were designed and synthesized by Beijing Tsingke Biotech (Beijing, CHN). Real-time PCR was conducted using the 2 \times SG Fast qPCR Master Mix (B639271, Sangon, CHN) and CFX Connect Real-Time PCR Detection System (BioRad). β -actin was used as an internal control to normalize individual gene expression levels. The relative expression of each target gene was calculated based on the $2^{-\Delta\Delta Ct}$ method.

The primer sequences are shown in Table 1.

2.16 | Western blot analysis analysis

For western blot analysis analysis, either cochlea was dissected or cells were harvested and then subjected to grinding. The total protein was extracted using the RIPA buffer (P0013B, Beyotime, CHN) and PMSF (ST506, Beyotime, CHN), and the total protein concentration was measured using the BCA Protein Assay Kit (23250, Thermo

TABLE 1 Primers used in this study.

Gene	Primer sequences (5'-3')
β -actin	Forward: CCATCATGAAGTGTGACGTTGAC Reverse: CCACCGATCCACACAGAGTACTT
Superoxide dismutase (SOD)	Forward: CGATGAAAGCGGTGTGCG Reverse: TGCACTGGTACAGCCTTGTGT
Catalase (CAT)	Forward: CTTCTGGAGTCTTCGTCGCC Reverse: TGCCCTGGTCGGTCTTGTA
Glutathione peroxidase (GPX)	Forward: TCAGTTCGGACACCAGGAGA Reverse: GTAA AGAGCGGGTGAGCCTT
Glutamate cysteine ligase (GCL)	Forward: CAGTGCGGTGAGACAATGAAG Reverse: GCCACTCGAGGCACTTTTTC

Scientific). The cell and tissue lysates were resolved by SDS-PAGE-Sample Loading Buffer 5× (P0015, Beyotime, CHN) and transferred to a polyvinylidene difluoride (PVDF) membrane (IPVH00010, Merck, GER). The membranes were blocked in NcmBlot Blocking Buffer (P30500, Ncm Biotech, CHN) for 30 min at room temperature and incubated with primary antibodies at 4°C overnight. Subsequently, the membranes were washed with TBST three times for 10 min each time and incubated with secondary antibodies for 2 h at room temperature. They were then washed three times with TBST again. ECL Chemiluminescent Substrate Reagent Kit (Zhuangzhi Biology, CHN) was used to observe the bands. The bands were analyzed using the FUSION FX SPECTRA (Vilber, FR).

The antibodies are shown in Table 2.

2.17 | Statistical analysis

All experimental data were processed and analyzed using GraphPad Prism 9.5 (GraphPad Software) and IBM SPSS Statistics 27.0 (IBM Corporation). The data were presented as the mean ± SEM. Measurement data were expressed as mean ± SEM. Comparisons among multiple groups were conducted using one-way analysis of variance, with Dunnett's or LSD-t test used for comparisons between groups. Statistical significance was set at $p < .05$.

3 | RESULTS

3.1 | Auditory function in mice with HHL is significantly impaired and SRT1720 reverses this change

Our initial investigations in HHL mice revealed that alterations in auditory function, such as changes in the auditory threshold, were most prominent on Day 1 following noise exposure, with partial recovery by Day 7 and complete recovery by Day 28. However, ABR

I wave amplitude, I wave latency, and ribbon synapses did not fully recover. Therefore, to assess the therapeutic effects of SRT1720 on HHL, we chose to conduct relevant auditory measurements on the first day following noise exposure. First, we measured the click-evoked ABR threshold in each group 1 d after noise exposure. The results show that solvent treatment had no significant effect on the ABR thresholds of mice (6.667 ± 1.054), noise exposure significantly elevated the ABR threshold (41.67 ± 2.108 , $p < .0001$), and re-treatment with SRT1720 markedly lowered the ABR threshold (10.83 ± 1.537) to levels not significantly different from the control group (5.833 ± 0.833) (Figure 1a). Then we compared the ABR thresholds at 1, 2, 4, and 8 kHz frequencies among different groups, and found that the thresholds of ABR at various frequencies exhibited the same trend as the click-evoked ABR threshold (Figure 1b). Additionally, the ABR I wave amplitude at 80 dB was calculated, showing that there was no significant difference between the VEHL group (8.573 ± 0.6234), SRT + NE group (11.23 ± 1.292), and the CON group (8.523 ± 0.252). However, the ABR I wave amplitude in the NE group decreased significantly (3.24 ± 0.455 , $p < .001$) (Figure 1c). The measurement of the latency of the ABR I wave at 80 dB showed no significant difference between the VEHL group (1.125 ± 0.028), SRT + NE group (1.088 ± 0.037), and the CON group (1.02 ± 0.021). But the latency in the NE group (1.387 ± 9.069) was higher than that of the CON group ($p < .01$). We also displayed the complete ABR test results of each group more intuitively in Figure 1e with four different colored curves, which are consistent with our previous findings. The results indicate that SRT1720 can significantly alleviate the auditory impairment in HHL mice, suggesting that SRT1720 has further research value.

3.2 | HHL mice showed ribbon synapse loss and abnormal stereocilia morphology and SRT1720 treatment had protective effects

In our previous study, we identified ribbon synapse loss as a major pathological change in HHL (Liu et al., 2022). To confirm the successful establishment of the HHL model and evaluate the protective effects of SRT1720, we used 4',6-diamidino-2-phenylindole (DAPI) to locate inner hair cells and a CtBP2 primary antibody to label ribbon synapses (shown as red fluorescent dots around inner hair cells) and observed changes in the ribbon synapses through quantitative analysis (Figure 2a-d). The basilar membrane of each mouse cochlea was divided into the apical, middle, and basal parts. The average number of ribbon synapses per IHC in the NE group was 7.833 ± 0.8433 in the apical part, 6.2 ± 0.7895 in the middle part, and 5.22 ± 0.4565 in the basal part. Each part showed a statistically significant decrease compared with the control group ($p < .01$). Round-window injection of SRT1720 before noise exposure mitigated ribbon synapse loss across all three parts ($p < .01$). No differences were observed in the number of ribbon synapses per IHC between the CON and VEHL groups. Therefore, we decided to disregard the effect of solvent

TABLE 2 Antibodies used in this study.

Antibody	Brand and Concentration
Rabbit anti-SIRT1	13161-1-AP, Proteintech, USA, 1:1000
Rabbit anti-p-SIRT1	AF3473, Affinity Bioscience, AUS, 1:1000
Rabbit anti-Nrf2	16396-1-AP, Proteintech, USA, 1:2000
Rabbit anti-NQO1	11451-1-AP, Proteintech, USA, 1:1000
Rabbit anti-HO-1	10701-1-AP, Proteintech, USA, 1:1000
Rabbit anti-GAPDH	10494-1-AP, Proteintech, USA, 1:5000
Mouse anti-LaminB 1	66095-1-Ig, Proteintech, USA, 1:20000
Mouse anti-Beta actin	66009-1-Ig, Proteintech, USA, 1:20000
goat anti-rabbit IgG	EK020, Zhuangzhi Biology, CHN, 1:2000
goat anti-mouse IgG	EK010, Zhuangzhi Biology, CHN, 1:2000

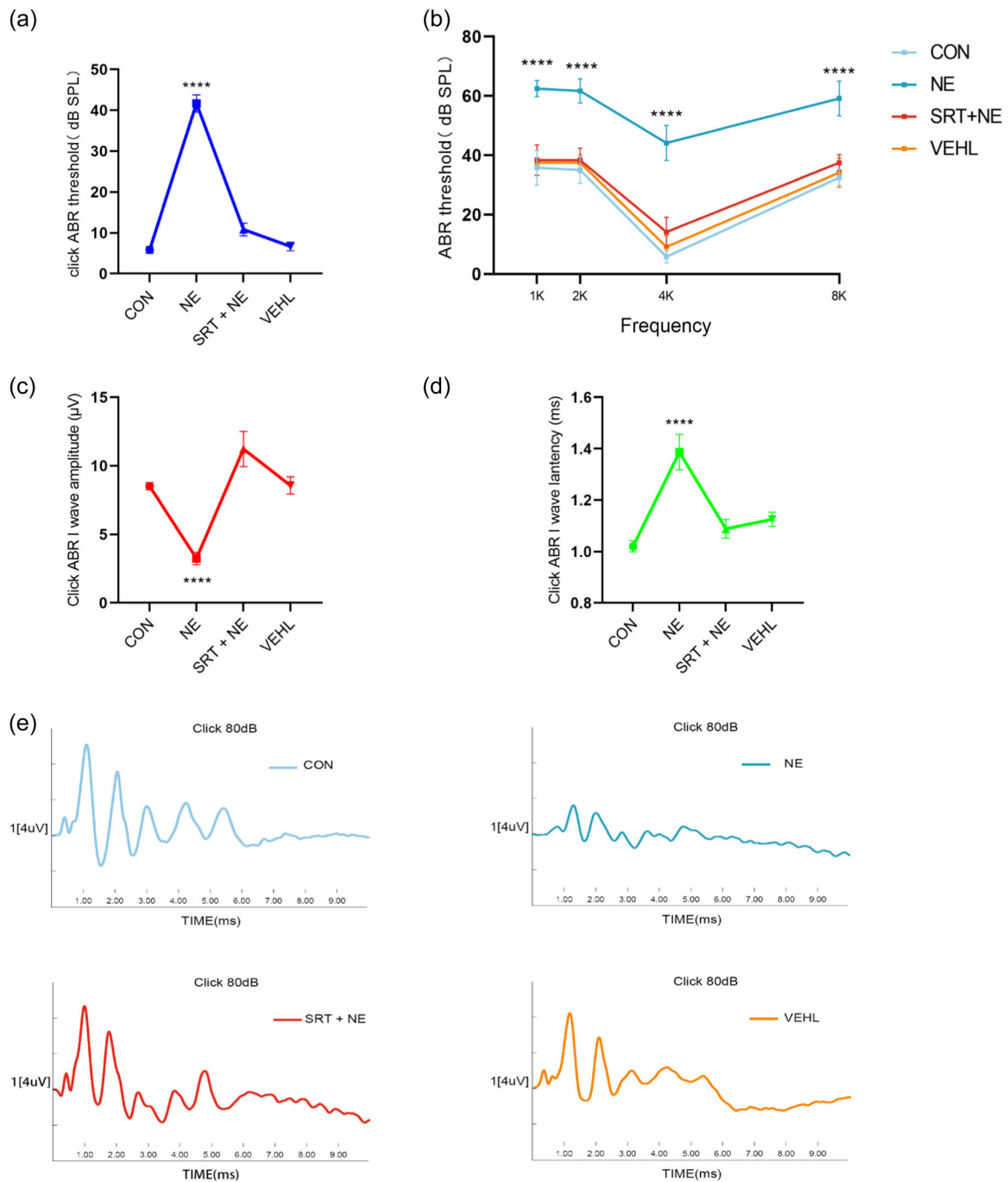


FIGURE 1 ABR testing for mice exposed to 110 dB military helicopter engine noise. (a) Click ABR threshold. (b) ABR thresholds at 1, 2, 4, and 8 kHz. (c) ABR I wave amplitude. (d) ABR I wave latency in each group of mice. (e) Click-evoked ABR waveforms of different groups recorded at 80 dB. $n = 6$, $*p < .05$, $**p < .01$, $***p < .001$, $****p < .0001$.

and primarily focus on the changes of the CON, NE, and SRT + NE groups in the following studies.

Since our previous research (Liu et al., 2022) and literature from other laboratories (Gilels et al., 2017; Xu et al., 2020) have demonstrated that NE can cause stereocilia disturbances, we observed the stereocilia changes in different parts of each group using scanning electron microscopy. Noise exposure caused substantial changes in the apical and middle parts, including instances of stereocilia lodging

and loss on some hair cell surfaces. After pretreatment with SRT1720 (SRT + NE group), stereocilia changes in the apical and middle parts of the basilar membrane were considerably reduced. However, compared with the CON group, some disordered stereocilia were still evident in the SRT + NE group, primarily concentrated in the apical part. The stereocilia in the bottom part of each group were relatively neatly arranged, potentially linked to the use of low-frequency noise as a stimulus in this study, given that hair cells in the basal part of the

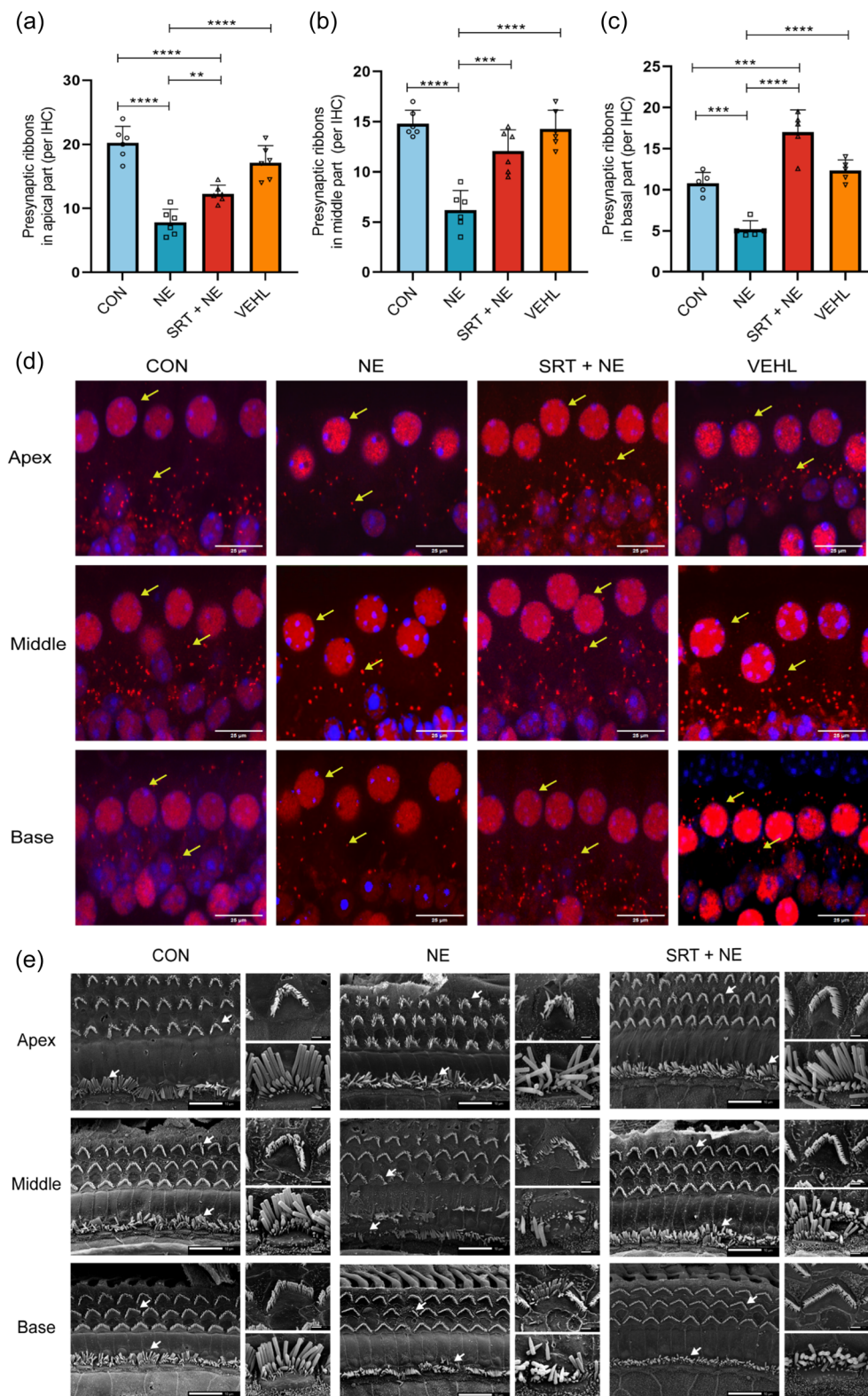


FIGURE 2 Changes of ribbon synapses per IHC and hair cell stereocilia. (a-c) Statistically analysis of ribbon synapse changes in the apical, middle, and bottom parts of the basilar membrane in each group. (d) Immunofluorescence images of ribbon synapse density changes in different turns of basilar membranes of the CON, NE, SRT + NE, and VEHL groups. Scale bar = 25 μ m. (e) Morphology of inner and outer hair cell stereocilia in the apical, middle, and basal part of the basilar membrane in each group. Scale bar = 10 μ m; enlarged image scale bar = 1 μ m. $n = 6$, * $p < .05$, ** $p < .01$, *** $p < .001$, **** $p < .0001$.

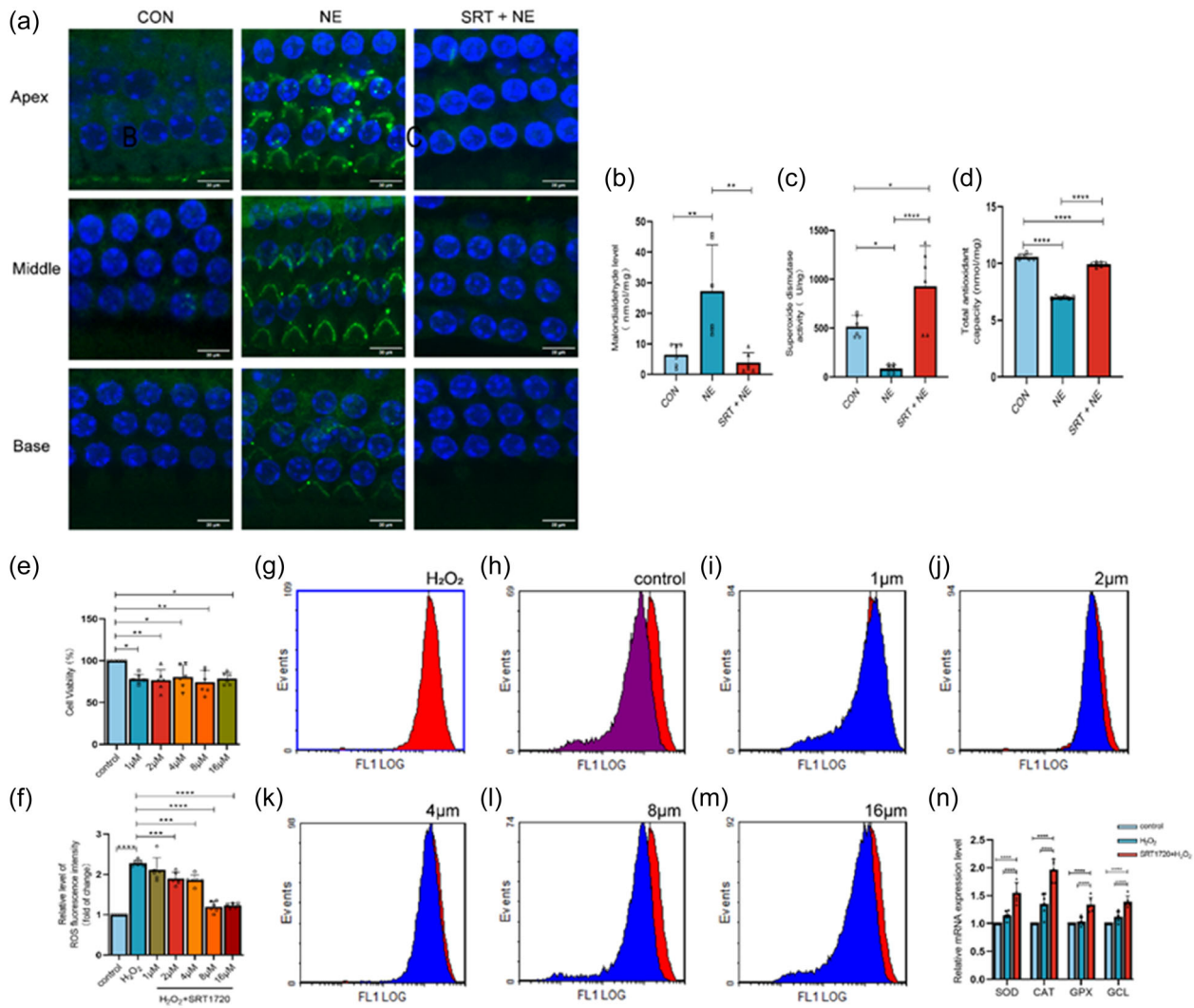


FIGURE 3 Changes in the products of oxidative stress in the cochlea of mice with HHL. (a) Immunofluorescence images showing changes in 4-HNE levels in the apical, middle, and basal parts of the basilar membrane in each group. Scale bar = 30 μ m. (b) MDA. (c) SOD activity. (d) T-AOC level changes in each group. (e) Cell viability in each group pretreated with different concentration gradients SRT1720 and H₂O₂. (f–m) ROS fluorescence in different groups via flow cytometry using DCFH-DA. (n) Relative expression of mRNA levels of SOD, CAT, GPX, and GCL in different groups. $n = 6$, * $p < .05$, ** $p < .01$, *** $p < .001$, **** $p < .0001$.

basilar membrane were mainly responsible for processing high-frequency sounds. No hair cell loss was observed in any group, which suggested that our HHL model is different from other types of hearing loss (Figure 2e).

3.3 | Oxidative stress exacerbates HHL and SRT1720 exhibits strong antioxidant effects

Previous study (Liu et al., 2022) has confirmed that oxidative stress injury is one of the main mechanisms underlying NIHL in guinea pig. Therefore, to prove that oxidative stress is an important factor in exacerbating HHL in mice and to determine whether SRT1720 can resist oxidative stress, we measured products of oxidative stress in different groups. Specifically, immunofluorescence staining revealed a higher

level of 4-HNE in the stereocilia of the outer hair cells after noise exposure, whereas it was considerably reduced after SRT1720 treatment (Figure 3a). Additionally, the MDA level increased from 6.427 ± 1.459 nmol/mg in the CON group to 27.22 ± 6.192 nmol/mg in the NE group ($p < 0.01$), whereas the SRT + NE group showed no significant difference compared with the CON group (Figure 3b). Besides, our findings indicated that the SOD activity was significantly lower in the NE group at 86.2 ± 16.7 U/ng compared to 516 ± 45.56 U/ng in the CON group and rose to 930.4 ± 166.9 U/ng in the SRT + NE group ($p < .05$) (Figure 3c). Similarly, the T-AOC levels were lower in the NE group than in the CON and SRT + NE groups ($p < .0001$) (Figure 3d). It can be seen that SRT1720 can alleviate various manifestations of HHL by mitigating oxidative stress-related damage. Therefore, we conducted further in vitro experiments to investigate the specific molecular mechanism of its reduction of oxidative stress damage.

We used H₂O₂ to construct an in vitro model of oxidative stress in HEI-OC1 cells. We tested different concentrations of SRT1720 (ranging from 1 to 16 μM) and verified their effects on cell viability using CCK8 (Figure 3e). The results showed that cell viability across all SRT1720 treated groups decreased to approximately 80% compared to that of the control group, with no significant differences among the various concentrations. We then measured mitochondrial ROS, a direct indicator of oxidative stress, and found that when treated with SRT1720 at a concentration of 8 μM, the reduction in ROS levels was more pronounced compared to that of lower concentrations and ROS levels decreased by approximately half compared to those in the H₂O₂ group ($p < .0001$), while no significant difference was observed compared to that in the 16 μM concentration; therefore, we chose this concentration for further mechanism research (Figure 3f–m). As for the expression of various antioxidants (SOD, CAT, GPX, and GCL) at the gene level, RT-qPCR results demonstrated higher antioxidant mRNA expression levels in the SRT1720 + H₂O₂ group than in the control and H₂O₂ groups ($p < .0001$) (Figure 3n). This further confirmed that SRT1720 alleviated oxidative stress both in vitro and in vivo. Given the influence of SRT1720 on the activation of SIRT1 by targeting it, our subsequent experiment focused on modifying the molecular pathway regulating oxidative stress anchored in SIRT1 and its downstream molecules.

3.4 | SIRT1/Nrf2 pathway may play a key role in the process of antioxidant stress

P-SIRT1 expression was assessed through western blot analysis, as the phosphorylation state reflects SIRT1 activation. The results showed significantly higher SIRT1 expression in the H₂O₂ group compared with that in the control group ($p < .0001$), however, it was still lower than that in the SRT1720 + H₂O₂ group ($p < .001$) (Figure 4a–c). This suggests that SIRT1 is activated and phosphorylated after oxidative stress in vitro and that SRT1720 significantly promotes its phosphorylation. Nrf2 regulates antioxidant gene expression by translocating to the nucleus to alter the cellular redox status. Western blot analysis of cytoplasmic proteins and nucleoproteins revealed a significant increase in nuclear Nrf2 levels in the SRT1720 + H₂O₂ group ($p < .005$) (Figure 4d–f). Confocal microscopy images also showed clear Nrf2 green fluorescence signals overlapping with the DAPI-stained nuclei (Figure 4g). Although the cytoplasmic Nrf2 content increased in the H₂O₂ group, no significant difference was observed in its nuclear expression compared to that in the control group ($p > .05$). And confocal microscopy did not reveal substantial nuclear Nrf2 enrichment. This indicates that SRT1720 inhibits Nrf2 degradation in the cytoplasm and promotes its translocation into the nucleus to perform antioxidant-related biological functions. This suggests that the process of SIRT1 activation by SRT1720 may be potentially linked to the translocation of Nrf2 into the nucleus to perform antioxidant-related biological functions.

To confirm that Nrf2 plays a key role in SRT1720's anti-oxidative stress effect, we transfected lenti-shNrf2 into HEI-OC1 cells to

knockdown Nrf2 expression. Western blot verification showed that while SRT1720 significantly promoted the expression of antioxidant proteins including NQO1 and HO-1 ($p < .05$), knocking down Nrf2 abolished this effect. Even in the Nrf2 knockdown group with SRT1720 treatment, no increase was observed in the expression levels of these antioxidant proteins compared to those of the H₂O₂ group (Figure 4h–l). In addition, we evaluated various oxidative stress parameters, including SOD activity, MDA levels, T-AOC, ATP production and MMP. The results showed that in the Nrf2 knockdown group stimulated with SRT1720 + H₂O₂ treatment, SOD activity was 43.93 ± 15.83 U/ng, whereas T-AOC was 29.09 ± 0.1801 nmol/mg, which was significantly lower than those in the control and SRT1720 + H₂O₂ groups ($p < .01$), however, T-AOC was higher than that in the H₂O₂ group ($p < .0001$) (Figure 4m,n). Correspondingly, the MDA level in the Nrf2 knockdown group was 3.258 ± 0.6043 nmol/mg, which was significantly higher than that in the control and SRT1720 + H₂O₂ groups, indicating that Nrf2 knockdown prevented SRT1720 from exerting its antioxidative stress effects (Figure 4o). Furthermore, the levels of ATP production and MMP were measured. The results indicated that when Nrf2 expression was normal, treatment with SRT1720 restored the decline in ATP production and MMP induced by H₂O₂ ($p < .0001$), whereas this protective effect was inhibited after Nrf2 knockdown ($p < .0001$) (Figure 4p–r).

4 | DISCUSSION

4.1 | Main interpretation

With the progress of social science, technology, and economic development, the use of a wide range of new equipment has made the hazard factors to which workers are exposed in their occupational activities increasingly complex. Long-term exposure to harmful noises is a common occupational risk worldwide (Tikka et al., 2017). Among the different noise frequencies, low-frequency noise has the greatest and most serious impact on occupational injuries (Berglund et al., 1996). Compared with other noise frequencies, low-frequency noise is more difficult to protect against, and regular exposure increases the risk of a variety of injuries in addition to hearing loss, including respiratory disorders (Verma et al., 2023), depression (Stansfeld, 1992), and cardiovascular diseases (Munzel et al., 2018). Military personnel (Moore, 2020), especially those in the air force, are at heightened risk of hearing loss because of factors such as the loud noise during takeoff and prolonged exposure to noisy environments without effective hearing protection devices. This exposure predominantly leads to low-frequency noise-induced hearing loss. A study from the United Kingdom (Moore, 2021) further supports this, revealing through retrospective research and analysis that veterans exposed to noise during their service, even if initially unaffected or experiencing only mild hearing loss, are more likely to experience accelerated and more severe hearing loss in the future compared to other individuals. This phenomenon has also been observed in the

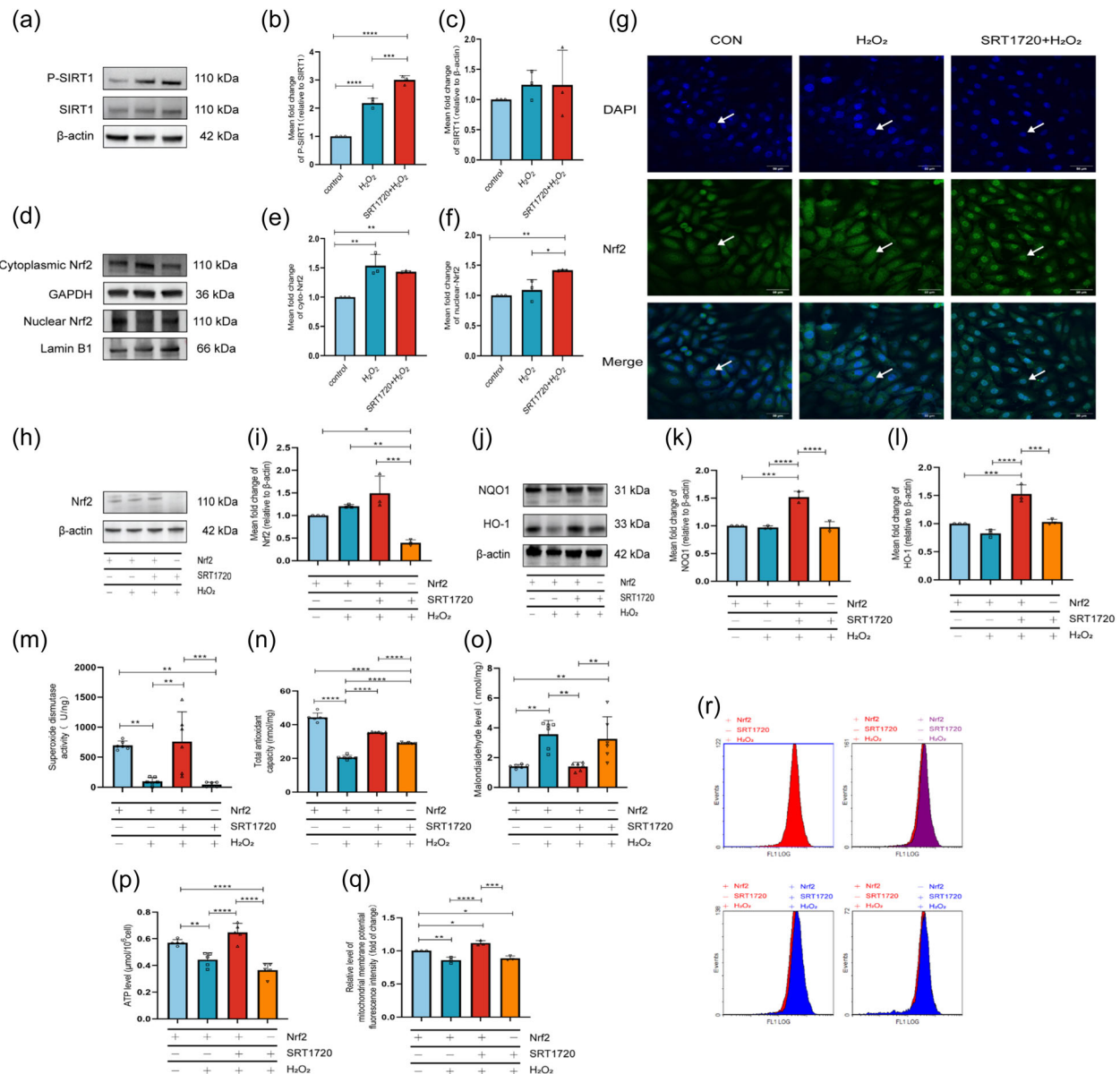


FIGURE 4 SIRT1/Nrf2 changes in response to oxidative stress. (a–c) Comparison of P-SIRT1 and SIRT1 expression levels in different groups. P-SIRT1 was normalized to SIRT1 expression, SIRT1 was normalized to β -actin expression. (d–f) Comparison of cytoplasmic Nrf2 and nuclear Nrf2 expression levels in different groups. (g) Nrf2 cytoplasmic nuclear translocation in different groups was detected via immunofluorescence staining using confocal microscopy. Scale bar = 50 μ m. (h–l) Comparison of NQO1, HO-1, and Nrf2 protein expression levels in different groups. (m–o) Comparison of SOD activity, MDA, and T-AOC levels in different groups (p) Comparison of ATP production levels in different groups. (q, r) Mitochondrial membrane potential (MMP) fluorescence intensity in different groups using Rhodamine 123. $n = 6$, * $p < .05$, ** $p < .01$, *** $p < .001$, **** $p < .001$.

general population, with approximately 1–10% of individuals exhibiting a normal hearing threshold but significant perceptual impairment in noisy environments (Hou et al., 2022; Qi et al., 2022). In addition, some patients with this type of symptom show age-related hearing loss in the young adult stage and are more sensitive to ototoxic drugs (Liberman & Kujawa, 2017). This phenomenon may be related to the permanent loss of the ribbon synapses between inner hair cells and type I spiral ganglion neurons (Schaeffe & McAlpine, 2011). This distinct type of hearing loss is also called HHL. In its early stages, HHL may cause mild or even undetectable damage

to the body. However, if left unaddressed, it can lead to severe consequences in the future, potentially surpassing the impact of NIHL. Currently, HHL lacks effective clinical diagnostic methods and treatment approaches, and its underlying pathogenesis remains unclear. Based on the high incidence of HHL in the population, which often goes unnoticed but profoundly affects long-term hearing health, and guided by the clinical principle of early diagnosis and intervention, our research group embarked on an extensive investigation into the causative factors of HHL and the molecular mechanisms implicated in its mitigation.

In this context, we previously successfully established a model of HHL in C57BL/6J male mice using noise exposure according to the clinical definition of HHL (Aedo & Aguilar, 2020; Wei et al., 2020; Yihong et al., 2024), which manifested as temporary shifts in ABR thresholds, irreversible ABR I-wave amplitude and latency reduction, and permanent decrease in ribbon synapses. Notably, in this study, we used broadband noise from the engine of a certain type of Chinese Air Force helicopter. We chose this type of noise for research mainly because of the special characteristics of the object it mainly affects, which is also one of the highlights of this study.

ABR is an auditory evoked potential induced by acoustic stimulation originating in the inner ear, auditory nerves, and brainstem. It records the nerve electrical activity on the scalp surface with a short latency of less than 10 ms (Liu et al., 2024). During our previous HHL modeling process (Liu et al., 2022), we observed that the ABR threshold increased, ABR I wave amplitude decreased, and I wave latency delay was most pronounced 1 d after NE. Although the hearing threshold gradually recovered after 2 weeks, the ABR I wave amplitude and latency did not recover until 4 weeks later. Recovery of the ABR threshold indicated that the hair cell bundles were unaffected. However, an unrecovered ABR I wave amplitude suggests an impairment in the sound-elicited discharge from the auditory nerve (Liu et al., 2019). Additionally, delayed ABR I wave latency reflects a decline in auditory signaling velocity because of the loss of ribbon synapses between inner hair cells and spiral ganglion cells (Liu et al., 2019). Our results indicated that, following NE, a decrease in the ABR I wave amplitude and delayed I wave latency was observed, consistent with previous findings, suggesting that lesions were located in the auditory nerve and ribbon synapses (Hou et al., 2022; Wei et al., 2020). The recoverable hearing threshold further suggested the absence of hair cell loss.

To assess the efficacy of SRT1720 in alleviating HHL, we evaluated various parameters, including ABR, ribbon synapse counts, stereocilia morphology, and detection of oxidative stress-related products 1 d after NE. These results showed that pretreatment with SRT1720 before NE improved the above parameters, indicating that SRT1720 can play an important protective role in alleviating HHL by reducing oxidative stress levels. For drug administration purposes, given that the blood-labyrinth barrier presence potentially reduces drug efficacy when administered systemically or orally, we chose the method of round window injection to direct the drug SRT1720 into the inner ear and allow it to take effect, this method has been proved to have no significant impact on hearing (Tan et al., 2019; Tao et al., 2022). In our *in vitro* experiments, we used H₂O₂ as a stimulating factor to induce oxidative stress in HEI-OC1 cells. We believe that conducting these *in vitro* experiments allowed us to study the role of SRT1720 in oxidative stress without the interference of other factors.

The pathogenesis of inner ear diseases is primarily associated with oxidative stress, chronic inflammation, and glutamate accumulation (Brozoski et al., 2013; Masuda et al., 2006; Verschuur et al., 2014). Excessive accumulation of ROS due to oxidative stress is a widely accepted cause of NIHL (Fetoni et al., 2019). While ROS play a

crucial physiological role in regulating protein phosphorylation and the redox homeostasis of transcription factors and ion channels (Fang et al., 2022), excessive ROS accumulation can lead to the continuous oxidation and destruction of proteins, lipids, and DNA (Ohlemiller et al., 1999). Two sources are often used to detect oxidative stress levels: markers of oxidative stress damage and antioxidants (Fetoni et al., 2008; Henderson et al., 2006; Kaya et al., 2015; Lee et al., 2015; Yamane et al., 1995). To reflect the degree of oxidative stress, we detected oxidative stress products, including ROS, lipid peroxides (MDA and 4-HNE), SOD, and T-AOC. T-AOC assessment involved measuring the reduction product Fe²⁺ to assess the overall content of diverse antioxidant enzymes as well as both large- and small-molecule antioxidants (Park et al., 2020; Wang et al., 2003; Wang et al., 2024). Additionally, we measured mitochondrial function indicators, such as MMP and ATP production levels, to reflect the degree of oxidative stress.

SIRT1 is one of the most widely studied NAD⁺ dependent histone deacetylase proteins in the sirtuin family (Frye, 1999). It plays a crucial role in various biological functions, such as the regulation of redox balance, inflammatory response, and energy metabolism. Moreover, SIRT1 has been studied in the field of hearing loss. Our previous study demonstrated high SIRT1 expression in the spiral ganglion, organs of Corti, and stria vascularis (Liu et al., 2022). Moreover, Xiong et al. (2015) showed that SIRT1 mitigates age-related hearing loss by interacting with the p53 and miR-34a pathways. Additionally, Hao et al. (2019) revealed that the miR-29b/SIRT1/PGC-1 α pathway can alleviate age-related hearing loss. Two earlier studies from our laboratory also indicated a significant protective role of SIRT1/PGC-1 α in NIHL and HHL models established in guinea pigs (Chen et al., 2020; Liu et al., 2022). Collectively, these findings suggest that SIRT1 exerts a protective effect against hearing loss through its antioxidative stress function. However, the use of the ginsenosides, Rd and resveratrol, in previous experiments resulted in the identification of numerous downstream targets, making it difficult to confirm their specificity for SIRT1 activation (Catalogna et al., 2019; Hubbard et al., 2013). Therefore, we selected SRT1720, a more specific SIRT1 agonist in this study to elucidate the crucial role of SIRT1 in HHL (Cao et al., 2013; Chao et al., 2022; Chauhan et al., 2011; Ichikawa et al., 2013). Our *in vitro* and *in vivo* results confirmed that SRT1720 effectively reduced the expression of oxidative stress damage markers, including ROS, MDA, and 4-HNE, while increasing the production of protective factors, such as SOD and T-AOC. Furthermore, it increased MMP levels and ATP production. In addition, SRT1720 significantly alleviated auditory system damage in HHL mice, including decreased hearing function, loss of ribbon synapses, and disorder of stereocilia.

Nrf2 is a crucial transcription factor responsible for maintaining redox balance within the body (Cuadrado et al., 2018). During oxidative stress, Nrf2 isolates from Keap1, inhibits its degradation, increases its translocation from cytoplasm to nucleus, and regulates the expression of its downstream antioxidant and detoxification genes, including NQO1 and HO-1 (Jaramillo & Zhang, 2013; Kansanen et al., 2012; Wang et al., 2004; Wei et al., 2020). Nrf2 is

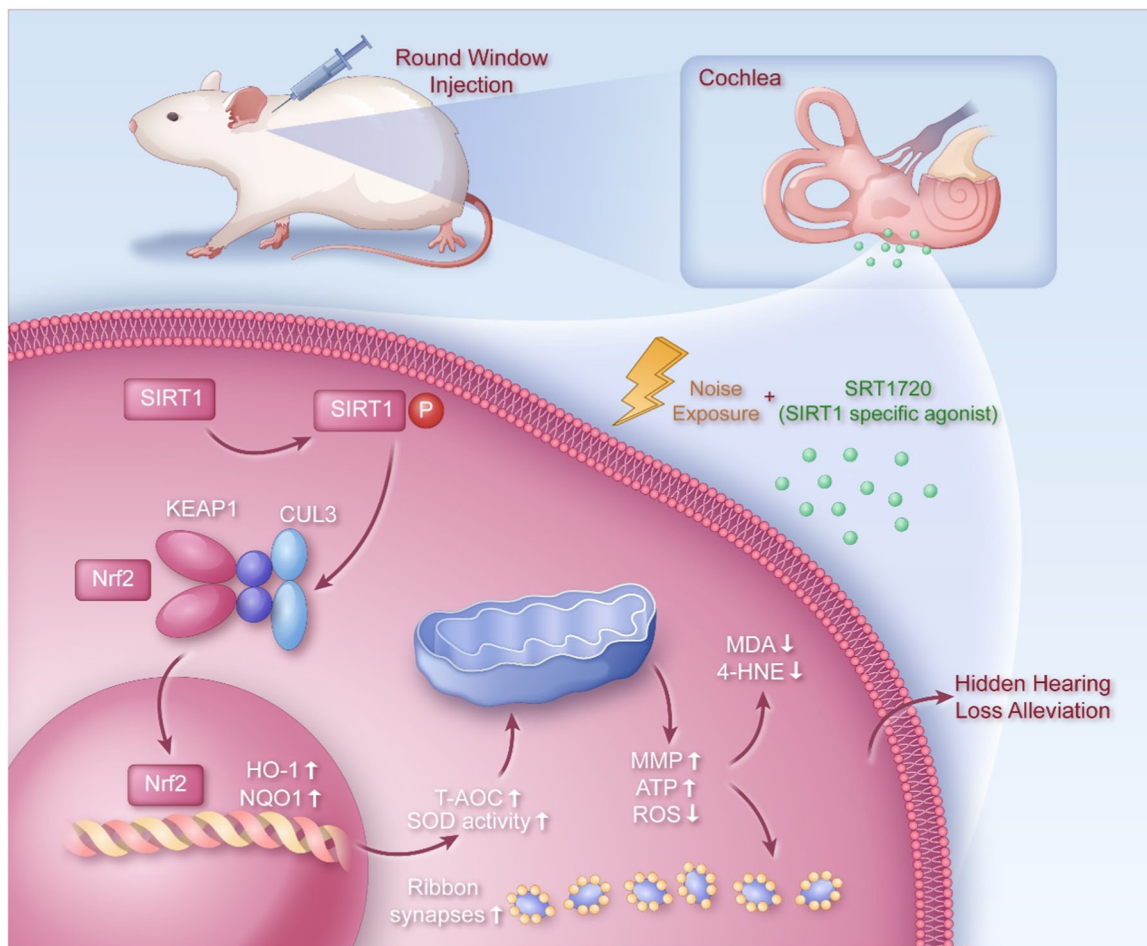


FIGURE 5 Schematic diagram of this study.

expressed throughout the body, including in the brain, retina, and inner ear. The expression of Nrf2 has been observed in all three turns (apex, middle, and base) of the organ of Corti; however, Nrf2 was not found to be significantly expressed in spiral ganglion cells or structures, such as the stria vascularis or Reissner's membrane (Li et al., 2021). Honkura et al. (Honkura et al., 2016) demonstrated that following NE, there was a slight increase in Nrf2 expression, and Nrf2 knockout significantly exacerbated noise-induced oxidative stress damage. This study also indicated that Nrf2 activation must be performed before NE to ensure sufficient promotion of downstream antioxidant production to maintain redox homeostasis. This was also the rationale behind our decision to administer SRT1720 before NE. Our results suggested that the SIRT1/Nrf2 pathway is an important molecular mechanism for attenuating the degree of oxidative stress injury and hearing loss in HHL mice, which has novel implications for the prevention and treatment of HHL.

4.2 | Limitations

Our study has some limitations. Firstly, the model used in this study may not fully reflect the clinical presentation of patients with HHL,

such as the most prominent feature of decreased speech recognition in noisy environments. Therefore, our future experiments will gradually shift focus from peripheral cochlear changes to central nervous system alterations to enhance clinical relevance. Secondly, our study exclusively investigated HHL based on the performance of male mice and did not consider the potential influence of other factors, such as estrogen, on HHL in female mice. Some studies suggest that estrogen may have a protective effect against hearing loss induced by NE (Wang et al., 2023) or following ovariectomy (Kim et al., 2021). Finally, as our research objects comprised animals and cells, we did not focus on solving the difficulty in the clinical diagnosis of HHL. We anticipate collaborating with other scientific researchers to develop more accurate clinical diagnostic measures for HHL to address this issue comprehensively.

5 | CONCLUSION

In summary, this study demonstrated that increased oxidative stress was the main pathogenic factor of impaired auditory function, ribbon synapse loss, and stereocilia morphology changes in a mouse model of HHL, and that this damage could be significantly alleviated by

antioxidative stress treatment. Additionally, SIRT1/Nrf2 may be the most important molecular mechanism for alleviating HHL by reducing oxidative stress. These findings deepen our understanding of HHL and offer new therapeutic targets for healthcare professionals and pharmaceutical researchers.

Schematic diagram of this study is shown in Figure 5.

AUTHOR CONTRIBUTIONS

Zeyu Zheng: Writing—original draft; writing—review and editing; data curation; formal analysis; investigation; methodology; project administration; software. **Peng Zhang:** Formal analysis; investigation; methodology; software. **Yang Fu:** Formal analysis; investigation; methodology; software. **Yihong Jiang:** Data curation; investigation. **Jing Zhu:** Data curation; investigation. **Fei Wang:** Formal analysis; visualization. **Shaoheng Li and Tian Li:** Investigation; methodology. **Zhuoru Zhang:** Investigation; visualization. **Tong Chang:** Formal analysis; visualization. **Min Zhang:** Conceptualization; methodology; investigation. **Bai Ruan:** Conceptualization; methodology; project administration; writing—review and editing. **Xiaocheng Wang:** Conceptualization; funding acquisition; methodology; supervision; validation; writing—review and editing.

ACKNOWLEDGMENTS

This work was supported by the National Natural Science Foundation of China [grant number 82373610]; the Military Medical Talents Support Fund of “Mount Everest Project” of Air Force Medical University, Military Logistics Scientific Research Standard [BKJ19B045]; Health Care Special Scientific Research Project of Health Bureau, Logistics Support Department, CMC [17BJZ24].

DATA AVAILABILITY STATEMENT

The data that support the findings of this study are available from the corresponding author upon reasonable request. All data are available at <https://www.jianguoyun.com/p/DTAO6HwQuaiFChi2kdMFIAA>.

ETHICS STATEMENT

All animal experiments conducted in this study were approved by the Institutional Animal Care and Use Committee of Xi'an Air Force Medical University, China (20230375).

ORCID

Tian Li  <http://orcid.org/0000-0002-8281-4459>

Xiaocheng Wang  <http://orcid.org/0009-0005-8220-1424>

REFERENCES

- Aedo, C., & Aguilar, E. (2020). Cochlear synaptopathy: New findings in animal and human research. *Reviews in the Neurosciences*, 31(6), 605–615. <https://doi.org/10.1515/revneuro-2020-0002>
- Berglund, B., Hassmén, P., & Job, R. F. S. (1996). Sources and effects of low-frequency noise. *The Journal of the Acoustical Society of America*, 99(5), 2985–3002. <https://doi.org/10.1121/1.414863>
- Brozoski, T. J., Wisner, K. W., Odintsov, B., & Bauer, C. A. (2013). Local NMDA receptor blockade attenuates chronic tinnitus and associated brain activity in an animal model. *PLoS One*, 8(10), e77674. <https://doi.org/10.1371/journal.pone.0077674>
- Cao, L., Liu, C., Wang, F., & Wang, H. (2013). SIRT1 negatively regulates amyloid-beta-induced inflammation via the NF- κ B pathway. *Brazilian Journal of Medical and Biological Research*, 46(8), 659–669. <https://doi.org/10.1590/1414-431X20132903>
- Catalogna, G., Moraca, F., D'Antona, L., Dattilo, V., Perrotti, G., Lupia, A., & Perrotti, N. (2019). Review about the multi-target profile of resveratrol and its implication in the SGK1 inhibition. *European Journal of Medicinal Chemistry*, 183, 111675. <https://doi.org/10.1016/j.ejmech.2019.111675>
- Chao, C. C., Huang, C. L., Cheng, J. J., Chiou, C. T., Lee, I. J., Yang, Y. C., & Huang, N. K. (2022). SIRT1/PGC-1 α as an SIRT1 activator for alleviating paraquat-induced models of Parkinson's disease. *Redox Biology*, 58, 102534. <https://doi.org/10.1016/j.redox.2022.102534>
- Chauhan, D., Bandi, M., Singh, A. V., Ray, A., Raje, N., Richardson, P., & Anderson, K. C. (2011). Preclinical evaluation of a novel SIRT1 modulator SRT1720 in multiple myeloma cells. *British Journal of Haematology*, 155(5), 588–598. <https://doi.org/10.1111/j.1365-2141.2011.08888.x>
- Chen, X. M., Ji, S. F., Liu, Y. H., Xue, X. M., Xu, J., Gu, Z. H., & Wang, X. C. (2020). Ginsenoside rd ameliorates auditory cortex injury associated with military aviation noise-induced hearing loss by activating SIRT1/PGC-1 α signaling pathway. *Frontiers in Physiology*, 11, 788. <https://doi.org/10.3389/fphys.2020.00788>
- C. Kohrman, D., Wan, G., Cassinotti, L., & Corfas, G. (2020). Hidden hearing loss: A disorder with multiple etiologies and mechanisms. *Cold Spring Harbor Perspectives in Medicine*, 10(1), a035493. <https://doi.org/10.1101/cshperspect.a035493>
- Cuadrado, A., Manda, G., Hassan, A., Alcaraz, M. J., Barbas, C., Daiber, A., Ghezzi, P., León, R., López, M. G., Oliva, B., Pajares, M., Rojo, A. I., Robledinos-Antón, N., Valverde, A. M., Guney, E., & Schmidt, H. H. W. (2018). Transcription factor NRF2 as a therapeutic target for chronic diseases: A systems medicine approach. *Pharmacol Rev*, 70(2), 348–383. <https://doi.org/10.1124/pr.117.014753>
- Fang, C., Xu, H., Yuan, L., Zhu, Z., Wang, X., Liu, Y., & Lou, M. (2022). Natural compounds for SIRT1-mediated oxidative stress and neuroinflammation in stroke: A potential therapeutic target in the future. *Oxidative Medicine and Cellular Longevity*, 2022, 1949718. <https://doi.org/10.1155/2022/1949718>
- Fetoni, A. R., Ferraresi, A., Greca, C. L., Rizzo, D., Sergi, B., Tringali, G., Piacentini, R., & Troiani, D. (2008). Antioxidant protection against acoustic trauma by coadministration of idebenone and vitamin E. *Neuroreport*, 19(3), 277–281. <https://doi.org/10.1097/WNR.0b013e3282f50c66>
- Fetoni, A. R., Paciello, F., Rolesi, R., Paludetti, G., & Troiani, D. (2019). Targeting dysregulation of redox homeostasis in noise-induced hearing loss: Oxidative stress and ROS signaling. *Free Radical Biology and Medicine*, 135, 46–59. <https://doi.org/10.1016/j.freeradbiomed.2019.02.022>
- Frye, R. A. (1999). Characterization of five human cDNAs with homology to the yeast SIR2 gene: Sir2-like proteins (sirtuins) metabolize NAD and may have protein ADP-ribosyltransferase activity. *Biochemical and Biophysical Research Communications*, 260(1), 273–279. <https://doi.org/10.1006/bbrc.1999.0897>
- Gilels, F., Paquette, S. T., Beaulac, H. J., Bullen, A., & White, P. M. (2017). Severe hearing loss and outer hair cell death in homozygous Foxo3 knockout mice after moderate noise exposure. *Scientific Reports*, 7(1), 1054. <https://doi.org/10.1038/s41598-017-01142-3>
- Hao, S., Wang, L., Zhao, K., Zhu, X., & Ye, F. (2019). Rs1894720 polymorphism in MIAT increased susceptibility to age-related hearing loss by modulating the activation of miR-29b/SIRT1/PGC-1 α signaling. *Journal of Cellular Biochemistry*, 120(4), 4975–4986. <https://doi.org/10.1002/jcb.27773>
- Henderson, D., Bielefeld, E. C., Harris, K. C., & Hu, B. H. (2006). The role of oxidative stress in noise-induced hearing loss. *Ear & Hearing*, 27(1), 1–19. <https://doi.org/10.1097/O1.aud.0000191942.36672.f3>

- Honkura, Y., Matsuo, H., Murakami, S., Sakiyama, M., Mizutari, K., Shiotani, A. & Motohashi, H. (2016). NRF2 is a key target for prevention of noise-induced hearing loss by reducing oxidative damage of cochlea. *Scientific Reports*, 6, 19329. <https://doi.org/10.1038/srep19329>
- Hou, S., Zhang, J., Wu, Y., Junmin, C., Yuyu, H., He, B. & Li, S. (2022). FGF22 deletion causes hidden hearing loss by affecting the function of inner hair cell ribbon synapses. *Frontiers in Molecular Neuroscience*, 15, 922665. <https://doi.org/10.3389/fnmol.2022.922665>
- Hubbard, B. P., Gomes, A. P., Dai, H., Li, J., Case, A. W., Considine, T., Riera, T. V., Lee, J. E., E, S. Y., Lamming, D. W., Pentelute, B. L., Schuman, E. R., Stevens, L. A., Ling, A. J. Y., Armour, S. M., Michan, S., Zhao, H., Jiang, Y., Sweitzer, S. M. & Sinclair, D. A. (2013). Evidence for a common mechanism of SIRT1 regulation by allosteric activators. *Science*, 339(6124), 1216–1219. <https://doi.org/10.1126/science.1231097>
- Ichikawa, T., Hayashi, R., Suzuki, K., Imanishi, S., Kambara, K., Okazawa, S., Inomata, M., Yamada, T., Yamazaki, Y., Koshimizu, Y., Miwa, T., Matsui, S., Usui, I., Urakaze, M., Matsuya, Y., Sasahara, M., & Tobe, K. (2013). Sirtuin 1 activator SRT1720 suppresses inflammation in an ovalbumin-induced mouse model of asthma. *Respirology*, 18(2), 332–339. <https://doi.org/10.1111/j.1440-1843.2012.02284.x>
- Jaramillo, M. C., & Zhang, D. D. (2013). The emerging role of the Nrf2-Keap1 signaling pathway in cancer. *Genes & Development*, 27(20), 2179–2191. <https://doi.org/10.1101/gad.225680.113>
- Kansanen, E., Jyrkkänen, H. K., & Levenon, A. L. (2012). Activation of stress signaling pathways by electrophilic oxidized and nitrated lipids. *Free Radical Biology and Medicine*, 52(6), 973–982. <https://doi.org/10.1016/j.freeradbiomed.2011.11.038>
- Kaya, H., Koç, A. K., Sayın, I., Güneş, S., Altıntaş, A., Yeğin, Y., & Kayhan, F. T. (2015). Vitamins A, C, and E and selenium in the treatment of idiopathic sudden sensorineural hearing loss. *European Archives of Oto-Rhino-Laryngology*, 272(5), 1119–1125. <https://doi.org/10.1007/s00405-014-2922-9>
- Kim, M. T., Lee, J. H., Carpena, N. T., Lee, M. Y., Chung, P. S., & Jung, J. Y. (2021). Estrogen replacement reduces hearing threshold shifts and cochlear hair cell loss after acoustic overexposure in ovariectomized rats. *Clinical and Experimental Otorhinolaryngology*, 14(1), 61–68. <https://doi.org/10.21053/ceo.2019.01662>
- Lee, S. H., Kim, H. S., An, Y. S., Chang, J., Choi, J., & Im, G. J. (2015). Protective effect of resveratrol against cisplatin-induced ototoxicity in HEI-OC1 auditory cells. *International Journal of Pediatric Otorhinolaryngology*, 79(1), 58–62. <https://doi.org/10.1016/j.ijporl.2014.11.008>
- Li, D., Zhao, H., Cui, Z. K., & Tian, G. (2021). The role of Nrf2 in hearing loss. *Frontiers in Pharmacology*, 12, 620921. <https://doi.org/10.3389/fphar.2021.620921>
- Lieberman, M. C., & Kujawa, S. G. (2017). Cochlear synaptopathy in acquired sensorineural hearing loss: manifestations and mechanisms. *Hearing Research*, 349, 138–147. <https://doi.org/10.1016/j.heares.2017.01.003>
- Liu, H., Lu, J., Wang, Z., Song, L., Wang, X., Li, G. L., & Wu, H. (2019). Functional alteration of ribbon synapses in inner hair cells by noise exposure causing hidden hearing loss. *Neuroscience Letters*, 707, 134268. <https://doi.org/10.1016/j.neulet.2019.05.022>
- Liu, J., Stohl, J., & Overath, T. (2024). Hidden hearing loss: fifteen years at a glance. *Hearing Research*, 443, 108967. <https://doi.org/10.1016/j.heares.2024.108967>
- Liu, Y. H., Jiang, Y. H., Li, C. C., Chen, X. M., Huang, L. G., Zhang, M. & Wang, X. C. (2022). Involvement of the SIRT1/PGC-1 α signaling pathway in noise-induced hidden hearing loss. *Frontiers in Physiology*, 13, 798395. <https://doi.org/10.3389/fphys.2022.798395>
- Masuda, M., Nagashima, R., Kanzaki, S., Fujioka, M., Ogita, K., & Ogawa, K. (2006). Nuclear factor-kappa B nuclear translocation in the cochlea of mice following acoustic overstimulation. *Brain Research*, 1068(1), 237–247. <https://doi.org/10.1016/j.brainres.2005.11.020>
- Moore, B. C. J. (2020). Diagnosis and quantification of military noise-induced hearing loss. *The Journal of the Acoustical Society of America*, 148(2), 884–894. <https://doi.org/10.1121/10.0001789>
- Moore, B. C. J. (2021). The effect of exposure to noise during military service on the subsequent progression of hearing loss. *International Journal of Environmental Research and Public Health*, 18(5), 2436. <https://doi.org/10.3390/ijerph18052436>
- Münzel, T., Sørensen, M., Schmidt, F., Schmidt, E., Steven, S., Kröller-Schön, S., & Daiber, A. (2018). The adverse effects of environmental noise exposure on oxidative stress and cardiovascular risk. *Antioxidants & Redox Signaling*, 28(9), 873–908. <https://doi.org/10.1089/ars.2017.7118>
- Ohlemiller, K. K., McFadden, S. L., Ding, D. L., Flood, D. G., Reaume, A. G., Hoffman, E. K., Scott, R. W., Wright, J. S., Putcha, G. V., & Salvi, R. J. (1999). Targeted deletion of the cytosolic Cu/Zn-superoxide dismutase gene (Sod1) increases susceptibility to noise-induced hearing loss. *Audiology and Neurotology*, 4(5), 237–246. <https://doi.org/10.1159/000013847>
- Park, S., Jang, J. W., & Moon, E. Y. (2020). BAFF attenuates oxidative stress-induced cell death by the regulation of mitochondria membrane potential via Syk activation in Wil2-NS B lymphoblasts. *Scientific Reports*, 10(1), 11784. <https://doi.org/10.1038/s41598-020-68628-5>
- Qi, G., Shi, L., Qin, H., Jiang, Q., Guo, W., Yu, N., Han, D., & Yang, S. (2022). Morphology changes in the cochlea of impulse noise-induced hidden hearing loss. *Acta Oto-laryngologica*, 142(6), 455–462. <https://doi.org/10.1080/00016489.2022.2086706>
- Schaette, R., & McAlpine, D. (2011). Tinnitus with a normal audiogram: physiological evidence for hidden hearing loss and computational model. *The Journal of Neuroscience*, 31(38), 13452–13457. <https://doi.org/10.1523/JNEUROSCI.2156-11.2011>
- Schubert, N. M. A., Reijntjes, D. O. J., van Tuinen, M., Vijayakumar, S., Jones, T. A., Jones, S. M., & Pyott, S. J. (2024). Pathophysiological processes underlying hidden hearing loss revealed in Kcnt1/2 double knockout mice. *Aging Cell*, 23, e14243. <https://doi.org/10.1111/accel.14243>
- Stansfeld, S. A. (1992). Noise, noise sensitivity and psychiatric disorder: epidemiological and psychophysiological studies. *Psychological Medicine Monograph Supplement*, 22, 1–44.
- Tan, F., Chu, C., Qi, J., Li, W., You, D., Li, K., Chen, X., Zhao, W., Cheng, C., Liu, X., Qiao, Y., Su, B., He, S., Zhong, C., Li, H., Chai, R., & Zhong, G. (2019). AAV- ie enables safe and efficient gene transfer to inner ear cells. *Nature Communications*, 10(1), 3733. <https://doi.org/10.1038/s41467-019-11687-8>
- Tan, W., & Song, L. (2023). Role of mitochondrial dysfunction and oxidative stress in sensorineural hearing loss. *Hearing Research*, 434, 108783. <https://doi.org/10.1016/j.heares.2023.108783>
- Tao, Y., Liu, X., Yang, L., Chu, C., Tan, F., Yu, Z., Ke, J., Li, X., Zheng, X., Zhao, X., Qi, J., Lin, C. P., Chai, R., Zhong, G., & Wu, H. (2022). AAV- ie -K558R mediated cochlear gene therapy and hair cell regeneration. *Signal Transduction and Targeted Therapy*, 7(1), 109. <https://doi.org/10.1038/s41392-022-00938-8>
- Tikka, C., Verbeek, J. H., Kateman, E., Morata, T. C., Dreschler, W. A., & Ferrite, S. (2017). Interventions to prevent occupational noise-induced hearing loss. *The Cochrane Database of Systematic Reviews*, 7(7), 006396. <https://doi.org/10.1002/14651858.CD006396.pub4>
- Verma, H., Shah, J., Singh, A., Singh, S., Sharma, B., & Shukla, B. (2023). Audiological, phonatory and cardiac correlates of individuals exposed to low-frequency noise or at risk of vibroacoustic disease. *International Archives of Otorhinolaryngology*, 27(3), e478–e486. <https://doi.org/10.1055/s-0042-1750160>
- Verschuur, C., Agyemang-Prempeh, A., & Newman, T. A. (2014). Inflammation is associated with a worsening of presbycusis: evidence from

- the MRC national study of hearing. *International Journal of Audiology*, 53(7), 469–475. <https://doi.org/10.3109/14992027.2014.891057>
- Wang, W., Gao, C., Hou, X. Y., Liu, Y., Zong, Y. Y., & Zhang, G. Y. (2004). Activation and involvement of JNK1/2 in hydrogen peroxide-induced neurotoxicity in cultured rat cortical neurons. *Acta Pharmacologica Sinica*, 25(5), 630–636.
- Wang, X., Sharma, R. K., Gupta, A., George, V., Thomas, A. J., Falcone, T., & Agarwal, A. (2003). Alterations in mitochondria membrane potential and oxidative stress in infertile men: A prospective observational study. *Fertility and Sterility*, 80(Suppl.), 2844–2850. [https://doi.org/10.1016/s0015-0282\(03\)00983-x](https://doi.org/10.1016/s0015-0282(03)00983-x)
- Wang, X., Zheng, H., Yang, B., Zu, M., Wang, Z., Zhang, J., Zheng, F., Yang, M., Tong, M. C. F., Zhao, L., & Bai, W. (2023). Estrogen as a guardian of auditory health: Tsp1-CD47 axis regulation and noise-induced hearing loss. *Climacteric*, 18, 1–11. <https://doi.org/10.1080/13697137.2023.2287632>
- Wang, Z., Xu, T., Sun, Y., Zhang, X., & Wang, X. (2024). AMPK/PGC-1 α and p53 modulate VDAC1 expression mediated by reduced ATP level and metabolic oxidative stress in neuronal cells. *Acta Biochimica et Biophysica Sinica*, 56(2), 162–173. <https://doi.org/10.3724/abbs.2024012>
- Wei, M., Wang, W., Liu, Y., Mao, X., Chen, T. S., & Lin, P. (2020). Protection of cochlear ribbon synapses and prevention of hidden hearing loss. *Neural Plasticity*, 2020, 8815990. <https://doi.org/10.1155/2020/8815990>
- Xiong, H., Pang, J., Yang, H., Dai, M., Liu, Y., Ou, Y., Huang, Q., Chen, S., Zhang, Z., Xu, Y., Lai, L., & Zheng, Y. (2015). Activation of miR-34a/SIRT1/p53 signaling contributes to cochlear hair cell apoptosis: Implications for age-related hearing loss. *Neurobiology of Aging*, 36(4), 1692–1701. <https://doi.org/10.1016/j.neurobiolaging.2014.12.034>
- Xu, C., Ren, W., Zhang, Y., Zheng, F., Zhao, H., Shang, H., Guo, W., & Yang, S. (2020). KIT gene mutation causes deafness and hypopigmentation in Bama miniature pigs. *American Journal of Translational Research*, 12(9), 5095–5107.
- Yamane, H., Nakai, Y., Takayama, M., Konishi, K., Iguchi, H., Nakagawa, T., & Kawakatsu, C. (1995). The emergence of free radicals after acoustic trauma and strial blood flow. *Acta Oto-laryngologica Supplement*, 519, 87–92. <https://doi.org/10.3109/00016489509121877>
- Yihong, J., Min, Z., Jing, Z., Fei, W., Zeyu, Z., Yuhui, L. & Xiaocheng, W. (2024). Construction and evaluation of C57 mouse model of noise-induced hidden hearing loss in military aviation. *Journal of Air Force Medical University*, 45(02), 163–168.

How to cite this article: Zheng, Z., Zhang, P., Fu, Y., Jiang, Y., Zhu, J., Wang, F., Li, S., Zhang, Z., Chang, T., Li, T., Zhang, M., Ruan, B., & Wang, X. (2025). The Potential role of the SIRT1-Nrf2 signaling pathway in alleviating hidden hearing loss via antioxidant stress. *Cell Biology International*, 49, 262–276. <https://doi.org/10.1002/cbin.12264>